



Transworld Research Network
37/661 (2), Fort P.O.
Trivandrum-695 023
Kerala, India

Thermal Wave Physics and Related Photothermal Techniques: Basic Principles and Recent Developments, 2009: 99-123 ISBN: 978-81-7895-401-1 Editor: Ernesto Marín Moares

4. Recent developments in thermal wave interferometry for gas analysis

E Marín¹ and H Vargas²

¹*Centro de Investigación en Ciencia Aplicada y Tecnología Avanzada, Instituto Politécnico Nacional, Legaria 694, Colonia Irrigación, C.P. 11500, México D.F., México;* ²*Centro de Ciencia y Tecnología, Laboratorio de Ciencias Físicas Universidade Estadual do Norte Fluminense, Av. Alberto Lamego 2000, Campos dos Goytacazes, RJ 28015-620, Brazil*

Abstract. The knowledge of thermal properties is of great importance due to their incidence in many aspects of our daily lives and in any system where heat transfer plays an important role. There are several techniques that have been developed for their measurement. Among them the dynamical methods offers advantages respecting the static ones due to their possibilities for the measurement of parameters characterizing non-stationary heat flux such as thermal diffusivity and effusivity. When a sample is illuminated with intensity periodical modulated radiation beams, the resulting time varying sample's temperature is often denoted as a thermal wave. The thermal wave model has demonstrated to be very useful for the description of the so called photothermal techniques, for which many variants exist. In particular the principles of thermal wave reflection and transmission at interfaces between media with dissimilar thermal properties, and their interference, have been used for the development of a technique named Thermal Wave Interferometry, whose basic principles and recent applications for the characterization of gaseous substances will be reviewed in this chapter.

Correspondence/Reprint request: Dr. E Marín, Centro de Investigación en Ciencia Aplicada y Tecnología Avanzada, Instituto Politécnico Nacional, Legaria 694, Colonia Irrigación, C.P. 11500, México D.F., México
E-mail: emarinm@ipn.mx

1. Introduction

It is well known that in many photothermal techniques the incoming intensity modulated light energy is converted into a series of thermal pulses, or thermal waves, which diffuse into the volume of the sample carrying information about some of its properties. There are several ways through which these waves can be detected and many models available for the interpretation of the experimental results. One of these models makes use of the analogy between thermal and genuine waves for the development of the so called thermal wave interferometry (TWI) technique, whose antecedents can be found in the pioneer work of Bennett and Patty [1] and whose basic principles, well described in the book of Almond and Patel [2], have been used in the past principally for coating characterization, particularly for thickness and thermal properties measurement [3-10]. The method assumes basically that the entire incident light energy is absorbed in the coating surface and converted into heat. The generated thermal waves will propagate towards the coating-substrate interface and back towards the coating surface. On striking the boundaries they will be partially reflected and transmitted occurring interference between the corresponding wave trains. The surface temperature is obtained by summing all the arriving waves or, in a straightforward manner, by solving the heat diffusion equations for each region of the multilayer system with the corresponding boundary conditions as in the well known Rosencwaig-Gersho Model [11]. One can show that the surface temperature depends on the thermal diffusion length and on the thickness of the coating, as well as on the thermal wave reflection coefficient at the coating-substrate interface, which is a function of the ratio of the thermal effusivities of the substrate and coating materials [2]. The thermal waves are detected mainly using an infrared detector allowing non-destructive and noncontacting measurements of the modulated thermal (blackbody) radiation emitted from the material surface. Evaluation of surface coatings by means of experiments based in periodically modulated heating have been performed by several authors, but less work have been performed in the field of TWI under transient (step) excitation of thermal waves, although observations [12, 13] made using transient techniques (such as Flash method [14]) may be attributed to the effect of internal multiple reflections between the interface and the substrate on the measured signal, as have been demonstrated elsewhere [15].

Although since the early eighties of the past century the TWI technique has been recognized as a well established tool for the characterization of solids, and new methodologies for data processing [16, 17] emerge regularly in the field, the concept of thermal wave interference has only gained

considerable attention for gas and liquid-phase applications after Shen and Mandelis [18] demonstrated the feasibility of detecting a thermal wave propagating across the gap formed between two walls, one acting as the generator and the other as a temperature sensor, showing the possibility of thermal property assessment for the material filling the cavity. As we will see later, the measured signal depends sensitively on the modulation frequency and the cavity length. Therefore length or frequency scans can be experimentally performed. It was demonstrated [19] that the cavity scanning mode offers several advantages because the frequency dependent instrumental transfer function remains constant during the experiment, thus fixing the noise bandwidth throughout the scan. The existence of extrema in both lock-in in-phase and quadrature channels, standing from the real and imaginary parts of the measured signal respectively, can be observed in both, frequency and cavity length scans. In the above mentioned works [18, 19] the authors have shown how the position of these extrema are related to the thermal diffusivity of the intracavity fluid allowing its determination with high accuracy and in a quick and easy way. That parameter can be also determined by fitting the theoretical expression to the experimental data. The relative difference between the thermal diffusivity values obtained by both methods is less than 0.5 % according to Shen, Mandelis and Ashe [20], who used 11th-order numerical polynomial fits to the experimental data in order to obtain an equation describing the experimental curve allowing the precise determination of the extrema positions. The precision of their results was demonstrated with measurements in several gases where the thermal diffusivities were obtained with fourth significant figures and with a great reproducibility, making perhaps the method as the most precise one to date for this purpose. One disadvantage of the extrema method could be the necessity of achieving sharp resonance peaks for precise measurements. Very low frequencies lead to strong signals but to flat peaks, while for high frequencies the peaks are quite sharp, but the signal-to noise ratio is compromised [20]. The fact that the mathematical formulas describing the extrema positions are similar to the antinodal conditions for standing waves in a pipe resonator have been lead to the concept of “thermal wave resonator cavity” widely used in early works by Mandelis and co-workers to design their experimental device, for which some applications were described in a recent published review [21] on thermal wave cavity with pyroelectric detection based devices. These applications are ranging from thermal diffusivity measurements in fluids and thermodynamic studies [22], to potential applications related to effective infrared (IR) emissivity measurements [23] in liquids by considering the thermal radiation emitted by the heated wall of the device in the theoretical model used to fit the

experimental data, among others. Radiation heat transfer inside the cavity was previously considered by the same group in the case of gaseous samples, allowing measurement of the IR emissivity of a thin film resistive metallic strip used as the source of thermal waves by means of its periodical Joule heating [24]. Bulk and surface optical absorption determination have been also demonstrated elsewhere [25] (particularly in Ti:Al₂O₃ crystals) using two cavities in the same thermal wave interferometric setup.

During the last decade several authors have proven the capabilities of the above described thermal wave resonator cavity method, denoted later “thermal wave interferometer” by Lima *et al* [26], to perform the thermal characterization of gases [27, 28], liquids [26, 29, 30] and their corresponding mixtures [31-33], and for kinetic studies of vapours diffusion in air [20, 34-37]. Similar configurations using photoacoustic (PA) detection (see later for details), instead of the pyroelectric one, have been also proposed [38-40]. The potential use of TWI for fuel analysis [41] has been recognized elsewhere [42]. An historical overview about thermal wave cavity developments in the last years can be found in [21].

In the present chapter we will show on the basis of several examples how a simple phenomenological theory leads to similar results as that based in a solution of the heat diffusion equations. We will make emphasis in the applications of thermal wave interference to the characterization of gases, highlighting those concerning the monitoring of hydrocarbon diffusion in air and its prospective use to the detection of fuels adulteration. It is worth to mention that despite the growing interest, the application of photothermal methods to gases thermal characterization, which is of considerable interest in several fields, for example in environmental studies, has remained limited, in comparison with studies in the liquid and solid phases. This is somewhat contradictory since the modern history of the PT science, before the well known works of Rosencwaig [11, 43, 44], began with the work of Viengerov [45] on opto- (photo) acoustic spectroscopy in gases, a field of considerable development today [46, 47]. Thermal wave interferometry has emerged as an extremely attractive technique in this direction.

2. Experimental details and basic phenomenological theory

In this section we will follow a phenomenological approach to describe the basic features of a thermal wave interferometer. In Fig. 1 is showed schematically a typical experimental set-up. It consists of a cavity of variable length containing a sample formed between a thin metallic foil (typically a 15 μm thick circular foil of Al with a diameter of 5mm [26]) and a temperature

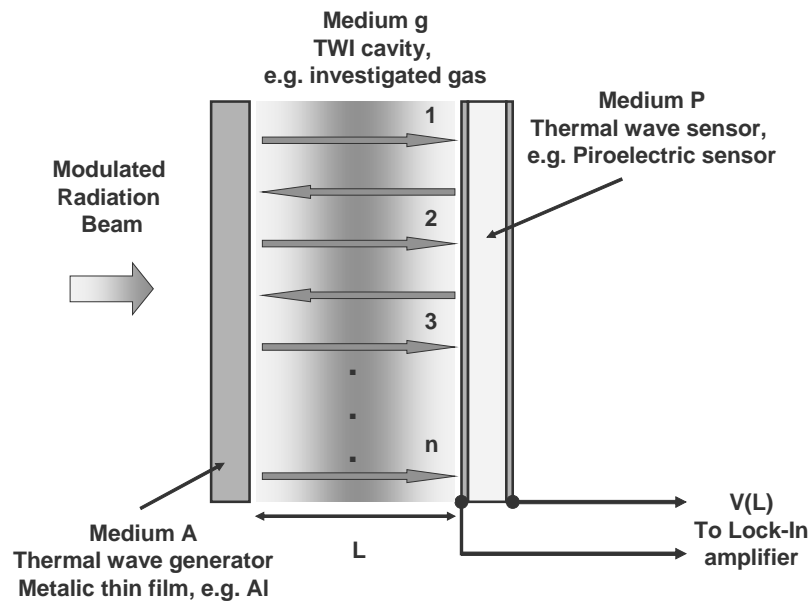


Figure 1. Schematic view of the thermal wave interferometer principle, showing the basics of thermal wave interferometry.

sensor. A laser light beam modulated by means of a mechanical chopper impinges on the black-painted outer surface of the metallic foil, which acts as a light absorber. Following the absorption of a modulated light beam, the foil temperature fluctuates periodically at the modulation frequency of the incident beam thereby launching a thermal wave into the gas filled cell (As mentioned in the introduction, in some early works an electrical heated metallic strip replaced the Al foil [24]). The thermal waves thus generated propagate back and forth between the foil and the sensor separated by a distance L . On striking the gas-foil and gas-sensor boundaries, the thermal waves are partially reflected, and interference between the reflected and incident wave trains will set in. The temperature oscillations resulting from the superposition of all arriving waves can be measured with the sensor as a function of the gas layer thickness.

The sensor is usually a 25 μm thick Photopyroelectric (PPE) sensor [48] consisting of a polyvinylidene difluoride (PVDF) polymer film with metalized surfaces serving as electrodes providing an output voltage, but a pyroelectric ceramic crystal (e.g., LiTaO_3) can be used as well. Some authors [38, 39] reported the use, as a sensor, of an Al foil coupled directly on the hole at the top of an electret microphone (Fig. 2) closing the (PA) air chamber in front of the electret diaphragm to get it hermetically sealed. The metallized electret diaphragm is connected through a resistor, R , to a metal plate separated from it by an air gap. The temperature variations at the Al foil resulting from the thermal wave interference described above induce pressure

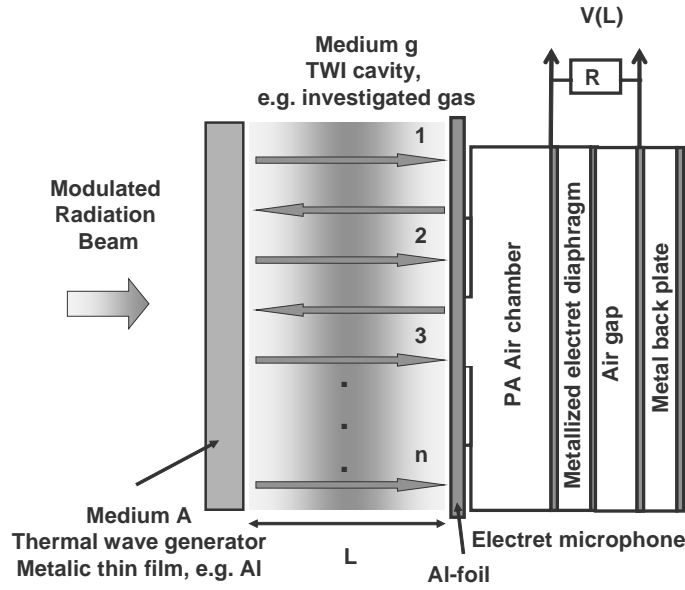


Figure 2. Schema of the TWI with photoacoustic sensing.

oscillations in the PA chamber which deflect the membrane, generating a voltage across the resistor, which is often supplied to a FET pre-amplifier already built in the microphone capsule. The measuring principle was then based in the so-called Open Photoacoustic Cell technique [49-53]. Bertolotti *et al* [54] reported about the use of a mirage technique [55] to prove the reflection and refraction of thermal waves at interfaces in a device similar to that of Fig. 1 with an oblique Al foil substituting the PE sensor.

The measured temperature can be estimated using the following phenomenological model [27]. Consider the situation depicted in Fig. 1. A gas layer of thickness, L , is sandwiched between the metallic foil and the sensor. The outer surface of the foil is heated uniformly (so that a one dimensional analysis will be valid) by a light source of periodically modulated intensity $I_0 (1 + \cos(\omega t))/2$, where I_0 is the light source intensity and $\omega = 2\pi f$ is the angular modulation frequency, acting as a thin superficial light absorbing layer on the surface of the cavity medium, which can be considered semi-infinite. The temperature distribution $T(x, t)$ within the cavity along the longitudinal x coordinate perpendicular to the Al foil surface, following the periodical heating, can be obtained by solving the heat diffusion equation with the boundary condition that the heat generated at the solid surface by light absorption is dissipated in the gas by diffusion. Accordingly, this solution can be written as

$$T(x, t) = \frac{I_0}{2\epsilon\sqrt{\omega}} \exp\left(-\frac{x}{\mu}\right) \exp\left[-i\left(\frac{x}{\mu} - \frac{\pi}{4} - \omega t\right)\right] = T_0 \exp(-qx) \exp(i\omega t) \quad (1)$$

i.e., a plane thermal wave, where ε is the thermal effusivity, $q=(i\omega/\alpha)^{1/2}$, α is the thermal diffusivity, $\mu=(2\alpha/\omega)^{1/2}$ represents the thermal wave diffusion length of the cavity material and $T_0=I_0/(2\varepsilon_g\omega^{1/2})$ is the temperature at $x=0$.

Consider now the propagation of a thermal wave described by Eq. (1) through the cavity medium (denoted by g) contained between the media A, corresponding to the metallic foil (a source) and P, corresponding to the sensor. The temperature at the surface $x=L$ is obtained by summing all the waves arriving at this point in the following way (for sake of simplicity, from now on we shall omit the term $\exp(i\omega t)$ in the calculations).

$$T(L) = T_1 + T_2 + \dots T_n = T_0 \left[e^{-qL} + R_{gA} R_{gP} e^{-3qL} + \dots + (R_{gA} R_{gP})^n e^{-(2n+1)qL} \right] \quad (2)$$

where R_{gA} and R_{gP} are the reflection coefficients at the corresponding interfaces (One can show that the reflection and transmission coefficients for the thermal wave at the interface, for normal incidence from region 1 to region 2, can be written as [8, 56-58]

$$R_{12} = \frac{1-b}{1+b} \quad (3)$$

and

$$T_{12} = \frac{2}{1+b} \quad (4)$$

respectively, where

$$b = \frac{\varepsilon_1}{\varepsilon_2} \quad (5)$$

is the ratio of the media thermal effusivities).

Summing up the geometric series in Eq. (2) one gets:

$$T(L) = T_0 \frac{\exp(-qL)}{1 - \gamma \exp(-2qL)} \quad (6)$$

where we have defined $\gamma=R_{gA}R_{gP}$.

The signal from the PPE or the PA sensor is proportional to the temperature given by the above equation. As mentioned in the introductory section, the instrumental transfer function is a function of the modulation frequency, but independent of L , making measurements as a function of L advantageous respecting those as a function of f , for which a normalization

procedure is in many cases impetuous. The complex signal is then sent to a Lock-In amplifier synchronized at the modulation frequency, where it is measured in the amplitude and phase or in the quadrature and in-phase channels. In the case of pyroelectric detection the output voltage can be then expressed as:

$$V(L) = V_0 \frac{\exp(-qL)}{1 - \gamma \exp(-2qL)} \quad (7)$$

where V_0 is a frequency dependent factor.

Theoretical expressions for the output signal, depending on the properties of the setup, materials, sensors, and cavity configuration, have been developed on a basis of straightforward calculations starting from the heat diffusion equations in each involved region of Fig. 1 [33, 59] for several measurement limits. For example, for the configuration described in Fig. 1, assuming a thermally thick PVDF pyroelectric sensor, one-dimensionality of the thermal wave field and neglecting heat losses by radiation and convection, Mandelis *et al* [59] obtained for the output PVDF voltage the following result:

$$V_{out} = V_a \left(\frac{\exp(-q_A L)}{1 - R_{gA}^2 \exp(-2q_A L)} \right) \left(\frac{\exp(-qL)}{1 - R_{gA} R_{gP} \exp(-2qL)} \right) \quad (8)$$

Here V_a depends on the modulation frequency and is also independent on cavity length. One can easily see that when a region A is thermally thin (as is the case of a thin Al foil with the thickness given above and for useful modulation frequencies for which $q_A L \ll 1$) the first term in parentheses is approximately equal to $1/(1 - R_{gA}^2)$, i.e. independent of both L and f , leading to a result similar to that obtained with the simple phenomenological model described above, i.e., Eq. (7). For the experimental situation in which the material of the cavity layer in the TWI cavity may be considered as thermally thick, that is, $q_g L \gg 1$, the pyroelectric sensor output voltage, as given by Eq. (7), reduces to:

$$V(L) = V_0 \exp(-qL) \quad (9)$$

so that its amplitude becomes

$$Amp(L, f) \approx \exp\left(-L \sqrt{\frac{\pi f}{\alpha}}\right) \quad (10)$$

and the phase:

$$\Delta\phi(L, f) \approx -L\sqrt{\frac{\pi f}{\alpha}} \quad (11)$$

In this case the thermal diffusivity can be obtained in a simple manner from the slope of the $\ln(\text{Amp})$ Vs. L (or $\ln(\text{Amp})$ Vs. $f^{1/2}$) curve or from the $\Delta\Phi$ Vs. L (or $\Delta\Phi$ Vs. $f^{1/2}$) plot [37]. This is often the situation when working with liquid samples of low thermal diffusivity. The result is quite similar to that used in the photopyroelectric technique in the direct or back configuration widely used for measurement of the thermal diffusivity of condensed matter samples [60-62] and detection of phase transitions [63-65]. Care must be taken when analysing limiting cases in TWI experiments with the fact that the product qL , determining the limit between thermally thin and thick regions, varies as the cavity length (and as the modulation frequency) does. For that reason we recommend the use of the more general expression to interpret the experimental results.

3. Thermal properties measurement in gases

There is an expanding demand for accurate and precise measurements of basic properties of a wide variety of gases generated by nature and modern industry, and in particular of thermal properties governing the heat conduction and diffusion in a given medium, such as thermal diffusivity and conductivity. In this direction TWI may become a valuable tool.

The Fig. 3 shows the results of a typical experiment performed with air as the material filling the cavity [21].

The In-Phase (In-P) and Quadrature (Q) Signal as a function of the cavity length were measured at a frequency of 10 Hz using a device similar to that shown in Fig. 1. Thermal waves were generated by the illumination of the Al foil with a 20 mW HeNe Laser.

One can see in both measurement channels the extrema corresponding to thermal wave resonance occurring when the phase of the thermal wave returns to its original value (plus an integral multiple of 2π) after one trip around the cavity [21]. The solid curves in the In-P and Q channels are the best fits of the data to the real and imaginary parts of Eq. (7), leading to a value of $\alpha=(0.219\pm 0.002)\text{cm}^2/\text{s}$ for the thermal diffusivity of air, in agreement with literature reported values [66, 67]. Following this methodology the thermal diffusivity of gases can be achieved with great precision.

Thermal diffusivity is related to other thermal properties such as the thermal conductivity, k , and thermal effusivity, ε , through the following relationships:

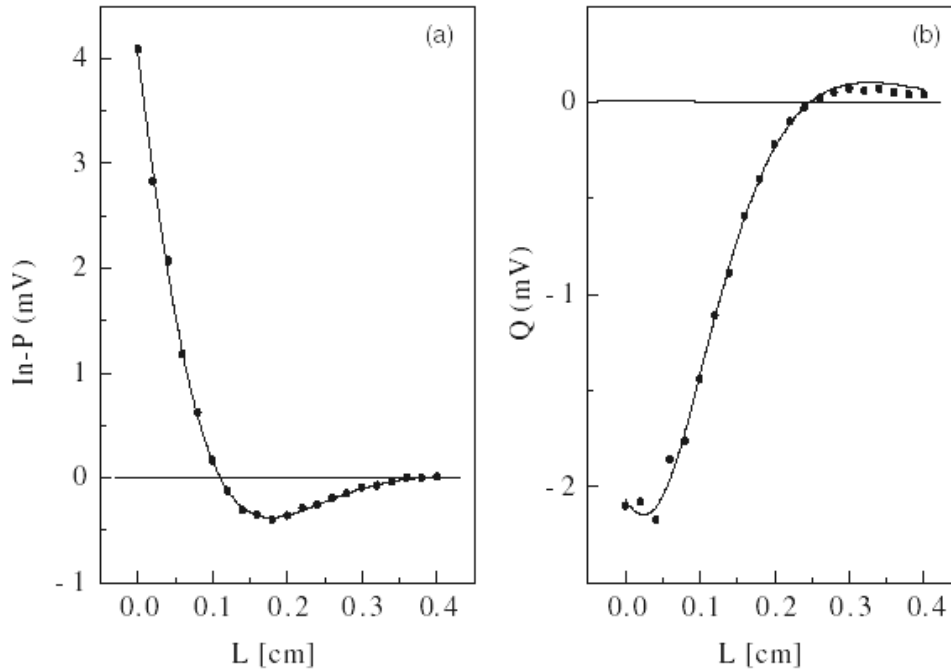


Figure 3. In-Phase and Quadrature signals as a function of the cavity length for air. The modulation frequency was 10 Hz. The solid curves are the best fit results to the Eq. (7) leaving V_0 and α as adjustable parameters (Reprinted with permission from [27] Copyright 2000, American Institute of Physics).

$$\alpha = \frac{k}{\rho c} = \left(\frac{\varepsilon}{\rho c} \right)^2 \quad (12)$$

where c is the specific heat and ρ is the density. The product $C=\rho c$ is the specific heat capacity or heat capacity per volume unit. To evaluate these properties for gases from a single TWI measurement two methods have been proposed, namely the method of mixtures [31, 32], and that based in a recent proposed device formed by a combination of a photoacoustic cell and a thermal wave interferometer in a single compact gas analyzer [28]. Next we will outline their basic principles.

3.1. The method of mixtures

The experimental setup, described in detail in Ref. [31], consists on a closed cell, adequately adapted for gas exchange and control of ambient parameters, in which the TWI is enclosed. The basics of the method proposed by Lima *et al* [31, 32] consists in carry out measurements, using the above outlined methodology, of the effective thermal diffusivity, α , of binary mixtures, as a function of the concentration, η , of the test gas (2) in a

reference one (1). The experimental data will be then fitted to the formula for the effective thermal diffusivity of the binary mixture of components 1 and 2 as predicted by effective medium theories. Among them [68, 69], the above mentioned authors have been resorted to the logarithm mixing model [69], which is more adequate for a random distribution of a two-phase system. Using Eq. (12) one can readily express the effective thermal diffusivity of the binary gas mixture in terms of the thermal properties of the constituent gases combining the equation for the effective thermal conductivity given by this model with the expression for the heat capacity per unit volume for the binary mixture. The result is [31, 32]:

$$\alpha = \alpha_1 \frac{\lambda^\eta}{1 + \left[\lambda \left(\frac{\alpha_1}{\alpha_2} \right) - 1 \right] \eta} \quad (13)$$

where

$$\lambda = \frac{k_2}{k_1} \quad (14)$$

Then, the parameters α_1 , α_2 and λ can be obtained as adjustable parameters from the fit of Eq. (13) to the experimental data. The parameter k_2 can be calculated using the well known k_1 value. (Note that thermal diffusivities can be also obtained by independent measurements performed in the separate components). The validity of the method was demonstrated before using pure gases of well known properties. The result of a typical measurement performed in CO₂-dry air mixtures is shown in Fig. 4. Table I summarize the results obtained for these and other high purity gases. From the thermal diffusivities and conductivities the volume heat capacities were calculated and compared with literature values taken from references [66, 67, 70, 71], showing a good agreement.

3.2. The photothermal gas (thermal) analyzer (PTGA)

Esquef *et al* [28] have described a simple and fast method for simultaneously measurements of the thermal diffusivity and effusivity. The basic design is represented schematically in Fig. 5 and consists of a cylindrical PA cell with microphone detection, filled with a reference gas (e.g. synthetic air) separated by an Al foil absorber (on which a modulated diode laser light beam impinges as shown in the figure) from a pyroelectric sensor through an 2mm thick gap. This gap between the Al foil and the sensor

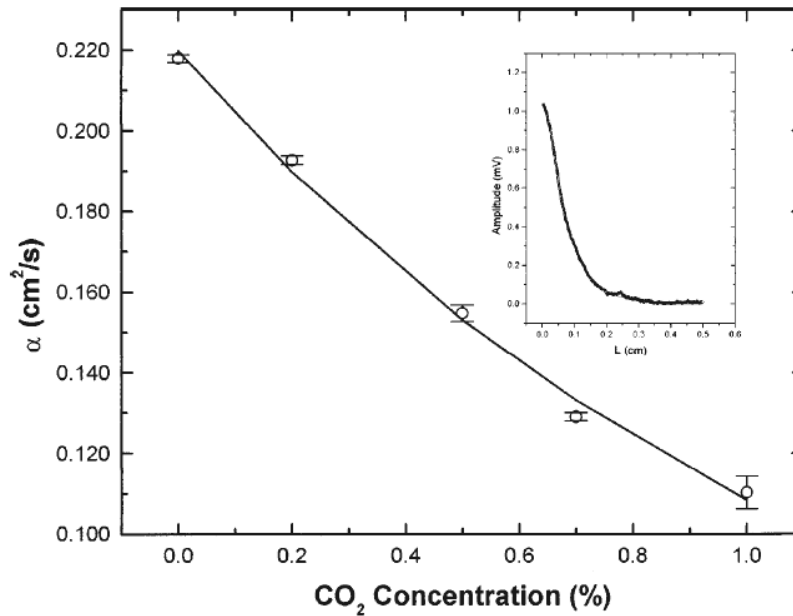


Figure 4. Thermal diffusivity as a function of the CO₂ concentration in dry air. The solid curve is the best fit of the data using the methodology outlined in the text. Inset: amplitude (calculated from the values of the in-P and Q voltages) of the TWI signal for a sample with 50% of each component as a function of the layer thickness. The solid curve is the result of data fitting to the amplitude of Eq. (7). Amplitude values were calculated from the In-P and Q signals, in which the presence of maxima and minima is helpful to observe differences in the curves corresponding to mixtures with similar concentrations. Reprinted with permission from [32] Copyright 2001, American Institute of Physics.

Table I. Thermal properties of gases measured using the method of mixtures. For comparison literature values for the specific heat capacity were included (after [31]). Reproduced with permission from Institute of Physics, IOP).

Gas	α (cm ² /s)	k (mW/cmK)	C (mJ/cm ³ K)	C _{lit} (mJ/cm ³ K)
Air	0.219 ± 0.002	0.262 ± 0.010	1.20 ± 0.06	1.22
CO ₂	0.110 ± 0.001	0.167 ± 0.008	1.52 ± 0.08	1.58
CH ₄	0.239 ± 0.004	0.443 ± 0.020	1.85 ± 0.09	1.66
C ₂ H ₄	0.129 ± 0.001	0.251 ± 0.013	1.95 ± 0.10	1.97
N ₂	0.223 ± 0.001	0.270 ± 0.010	1.21 ± 0.06	1.21

constitutes a TWI pyroelectric (PE) cell. The entire system is enclosed in a temperature controlled gas reservoir, so that the TWI cavity can be filled with the gas one wants to characterize, the so-called active or test gas. It was shown that the PTGA allows measurement of the thermal diffusivity of the test gas through the TWI-PE cell and, simultaneously, the thermal effusivity using the PA cell, with an accuracy of 3% in both properties.

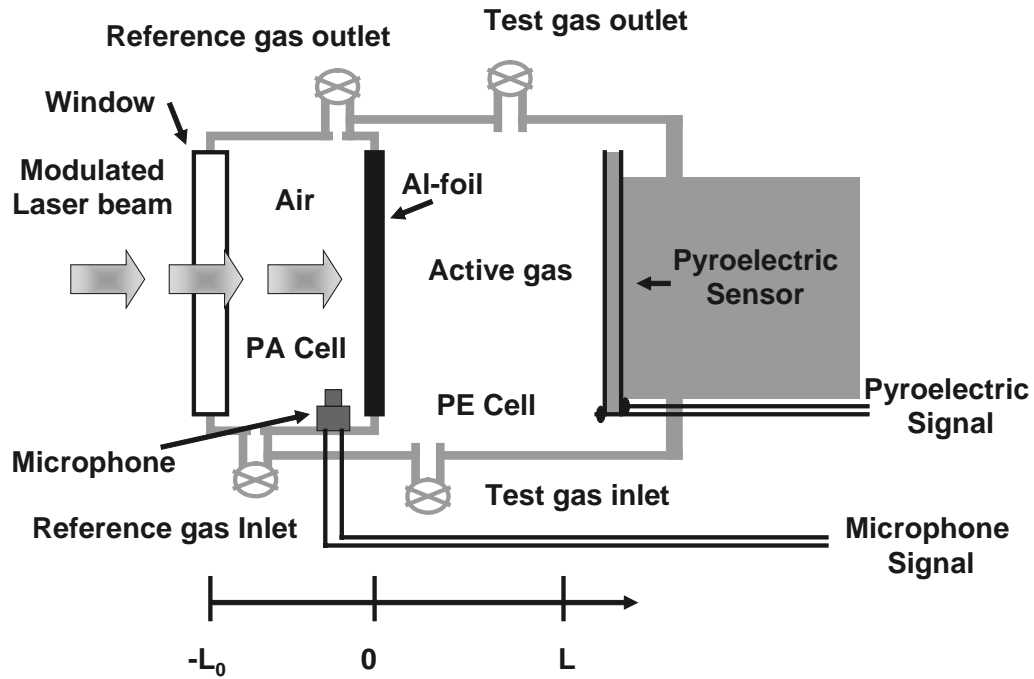


Figure 5. Schematic view of the experimental PTGA setup.

The principle of measurement can be described briefly as following: It is assumed that both test and reference gases are thermally thick for the used modulation frequency (this is valid for gases for a frequency $f=10\text{Hz}$ and gas lengths of about 2 mm). If the Al foil is thermally thin, then the output voltages of the microphone in the PA cell and of the PE sensor in the TWI (in the limiting case given by Eq. (10)), normalized with respect to the corresponding signals when the test cell is filled with the same gas as the reference, can be written as

$$S_{PA\text{norm}} = \frac{2}{1 + \frac{\varepsilon}{\varepsilon_0}}; \quad S_{PE\text{norm}} = \exp\left(-L \sqrt{\frac{\pi f}{\alpha_0}} \left(\sqrt{\frac{\alpha_0}{\alpha}} - 1\right)\right) \quad (15)$$

respectively. Here ε (ε_0) is the thermal diffusivity of active (reference) and L is the thickness of the TWI cavity.

The experimental procedure makes use of the above equations and consists of measuring both the PE and PA signals starting with both cells filled with the reference gas (at that point $S_{PA\text{norm}}=S_{PE\text{norm}}=1$) and, in sequence, acquiring the typical time evolution curves due to the exchanging of the reference gas with the active one at a controlled flow rate to a instant at which the TWI cavity is completely filled with the test gas and both signals reach constant saturation values corresponding to the values given by Eqs.

(15). From the saturation values of the PA and PE signals the thermal effusivity and diffusivity respectively of the test gas can be calculated if the corresponding values for the reference gas are well known.

In Fig. 6 a typical result obtained for synthetic air (20% O₂ and 80% N₂) as a reference and CO₂ (99.99%) as a test gas [28] is shown. Values of α and ε for CO₂ were obtained using Fig. 6 and Eqs. (15). The same was made for CH₄. These results are summarized in Table II.

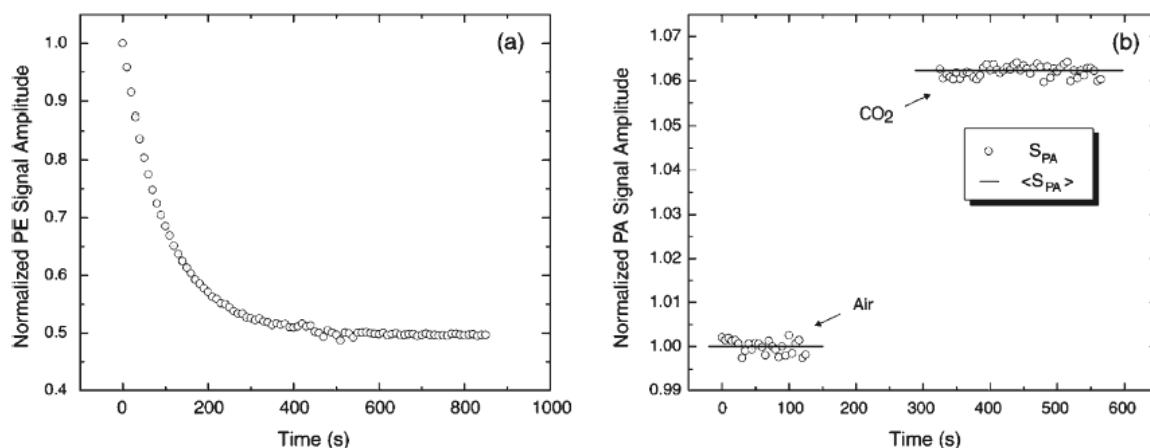


Figure 6. (a) Time evolution of the normalized PE signal amplitude and (b) PA signal amplitude during the synthetic air-CO₂ exchange. The modulation frequency was 10 Hz, the temperature was 23^oC and the test gas flow rate was 4 L/h. (Reprinted with permission from Ref. [28]. Copyright 2006 American Chemical Society).

Table II. Values of the thermal properties of gases using the PTGA method as determined in Ref. [28]. The thermal conductivity was calculated using Eq. (12) in order to compare the results with literature values [72, 73]. (Reprinted with permission from Ref. [28]. Copyright 2006 American Chemical Society).

Gas	α (cm ² /s)	ε (mWs ^{1/2} /cm ² K)	k (mW/cmK)	k_{lit} (mW/cmK)
CO ₂	0.109 ± 0.004	0.494 ± 0.007	0.163 ± 0.003	0.168
CH ₄	0.247 ± 0.002	0.681 ± 0.017	0.338 ± 0.006	0.334

4. Studies of hydrocarbon diffusion in air

One of the first applications of TWI aimed at the evaluation of the thermal diffusivity of air-hydrocarbon vapours mixtures [20, 27]. In these experiments a liquid portion of the liquid hydrocarbon sample is placed inside a closed cell in which the initially air filled TWI cavity of fixed length is assembled (Fig. 7).

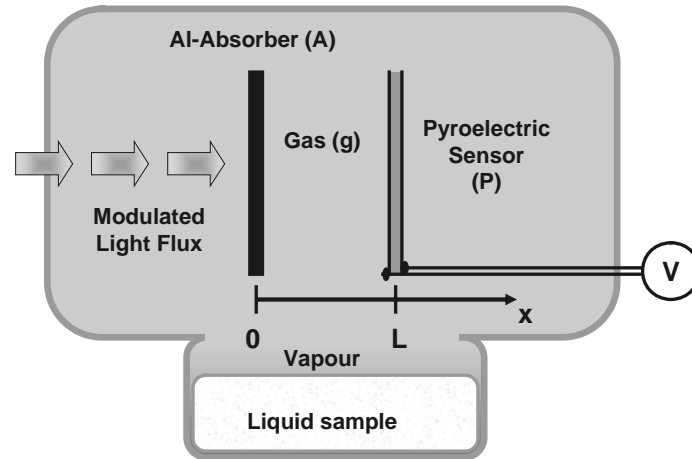


Figure 7. Schematic view of the TWI design for the study of mass diffusion of hydrocarbon vapours in air.

The hydrocarbon vapour resulting from the evaporation process diffuses into the air inside the cavity. As a result, the thermal properties of the resulting gas mixture change with time, following the changes of the vapour concentration in air. This process continues until saturation takes place, a moment at which one begins recording the signal as a function of the cavity length in order to measure the thermal diffusivity of the resulting mixture. With the aim of obtain a quantitative physical interpretation of the above described transient process, Lima *et al* [35] devised a method allowing the measurement of the mass diffusion coefficients of the hydrocarbon vapours in air, which can be potentially used to perform measurements in other gas species.

The model makes use of Eq. (9) by assuming that the TWI cavity is thermally thick for a fixed 2mm length and 10 Hz modulation frequency. In this case the normalized voltage represents the quotient of that measured when the saturation is reached and the initial value at $t=0$ when the cavity is only filled by air [35, 36]. For the thermal diffusivity α for the mixture of a concentration η of hydrocarbon vapour in air the logarithm mixing model was also selected and so Eq. (13) was used. To calculate the time dependence of the concentration the mentioned authors resorted to solve the well known mass diffusion equation (second Fick's Law) [74] with the boundary condition that the particle flux at the bottom of the gas column above the liquid reservoir of Fig. 7 is proportional to the concentration difference $\eta - \eta_0$, where η_0 is the hydrocarbon vapour saturation concentration. They demonstrated that the solution can be expressed as:

$$\eta = \eta_0 \left(1 - \exp\left(-\frac{t}{\tau}\right) \right) \quad (16)$$

where τ is the hydrocarbon vapour diffusion time defined as

$$\tau = \frac{L_C^2}{2D} \quad (17)$$

in which D is the mass diffusion coefficient and L_C is the characteristic length corresponding to the vertical gas column extending from the liquid level to the top of the cell, that was equal to 10cm. The derivation of Eq. (16) is presented with detail in the Appendix of Ref. [35].

Fig. 8 shows a typical time evolution of the TWI normalized signal amplitude for different air hydrocarbon mixtures carried out at ambient temperature (23°C) and pressure (760mm Hg) and within an ambient relative humidity of 60%. The solid curves are the result of the best fits by means of the described model, whose results are summarized in Table III.

Values of the thermal properties for the involved gases used in the fit were taken from Refs. [72, 75]. From the value of τ the mass diffusion coefficients were obtained using Eq. (17). Comparison with the literature reported values [75] shows a good agreement, indicating that the model provides an adequate description of the time signal behaviour and also the method is adequate for measurement of mass diffusion coefficients in gases.

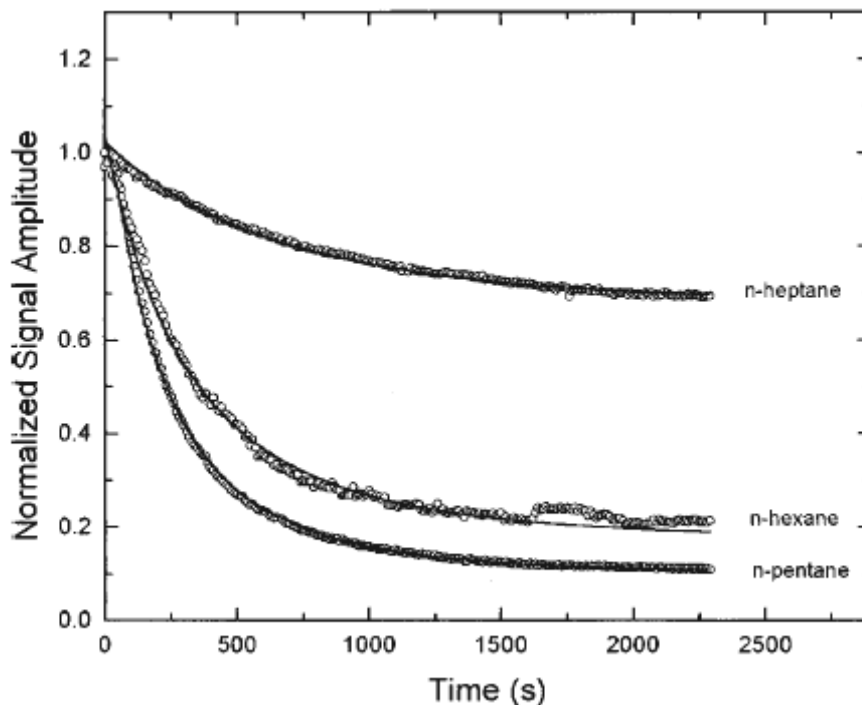


Figure 8. Time evolution of the normalized TWI signal amplitude for different hydrocarbon samples (Reprinted with permission from [35] Copyright 2002, American Institute of Physics).

Table III. Values of the fitting parameters η_0 and τ , and of the obtained diffusion coefficients for different hydrocarbons in air. (Reprinted with permission from [35] Copyright 2002, American Institute of Physics).

Hydrocarbon	η_0	τ (s)	D (cm ² /s)	D_{lit} (cm ² /s)
n-pentane	0.534 ± 0.002	581 ± 2	0.0861 ± 0.0004	0.0842
n-hexane	0.349 ± 0.001	702 ± 5	0.0713 ± 0.0006	0.0732
n-heptane	0.062 ± 0.001	793 ± 4	0.0630 ± 0.0002	0.0674

5. Characterization of automotive fuels

One possible application of the above mentioned methodology is the characterization of automotive fuels, a field of considerable attention today due to several reasons. In this section we will discuss the results of some developments in the areas of fuel evaluation by octane rating and fuel adulteration recognition. In the former case we will show how the TWI method can offer advantages respecting the well standardized motor methods. On the other hand, the incentive to monitoring retail fuels is very powerful because several studies estimated that a higher number of gasoline samples is adulterated in gas stations, mainly in developing countries, with the aim of increase the profits [42].

5.1. Octane rating

The octane rating of a spark ignition engine fuel is the knock resistance compared to a (arbitrary selected) mixture of isooctane and *n*-heptane. By definition, isooctane is assigned an octane rating of 100 and *n*-heptane is assigned an octane rating of zero. An 87-octane gasoline, for example, possesses the same anti-knock rating of a mixture of 87% (by volume) isooctane and 13% *n*-heptane. The most common type of octane rating worldwide is the Research Octane Number (RON). RON is determined by running the fuel in a test engine with a variable compression ratio under controlled conditions, and comparing these results with those for mixtures of isooctane and *n*-heptane. Another type of octane rating is the so-called Motor Octane Number (MON), which is a better measure of how the fuel behaves when it is under load. MON tests use the same engine to that used in RON testing, but with a preheated fuel mixture, a higher engine speed, and variable ignition timing to further stress the fuel's knock resistance. In some countries the headline number is the average of the RON and the MON, sometimes called the Anti-Knock Index (AKI), Road Octane Number (RdON), Pump Octane Number (PON), or $(R+M)/2$. The resulting figures of merit of this standard testing are known to be strongly linearly correlated to the fuels'

vapor thermodynamic properties such as, for instance, their vapor pressure. A correlation existing between the PON parameter and the fuels' vapor thermal diffusivities have been investigated recently using TWI [76, 77].

For example, Cardoso *et al* [76] used a method similar to that described in Section 4 consisting essentially of measuring the time evolution of the hydrocarbon mixtures vapors in an originally air-filled closed cell using a TWI. Liquid mixtures of isooctane and *n*-hexane (by volume) were prepared and 1cm³ of each sample was put in the recipient screwed at the cell bottom, as shown in Fig. 7.

Hydrocarbon vapor diffusion into the TWI cavity takes place after saturation is reached, a moment at which thermal diffusivity is measured using the cavity length scanning method. Typical In-P and Q curves are represented in the Fig. 9 for various relative concentrations of the hydrocarbons in the liquid samples.

Note the shift of the curves when the concentration is varied. It is worth to mention that although *n*-heptane is used as one of the primary references for octane definition, *n*-hexane was used in the here refereed works because it showed a more accentuated dependence of thermal diffusivity as a function of the mixture relative concentrations.

From these curves the thermal diffusivity was calculated by fitting using Eq. (7). The corresponding values are shown in Fig. 10 as a function of the PON number, determined using the motor method [78, 79]. The solid curve is the best fit to a first order exponential function performed in order to show that a correlation exists between both parameters.

The existence of a correlation has been instigating research work to seek the development of an alternative low-cost method aimed at gaining in accuracy, and of a portable device for field applications.

5.2. Fuel adulteration measurements

As mentioned above, in many parts of the world the adulteration of automotive fuels with lower priced materials is a widespread practice. Apart from the suboptimal performance of transportation fuels, and the consequent damage to the engines in itself, this commercial malpractice increases considerably the environment pollution, the potential human toxicity if frequently skin contact is allowed, and the premature failure of components in the fuel systems, among others. But in many cases gasoline may well continue to meet all specifications and would not exhibit drive ability problems if "judicious" adulteration is performed [41].

Taken these facts in mind Lima *et al* [41] used the same method as in the previous section for the measurement of both the characteristic time for

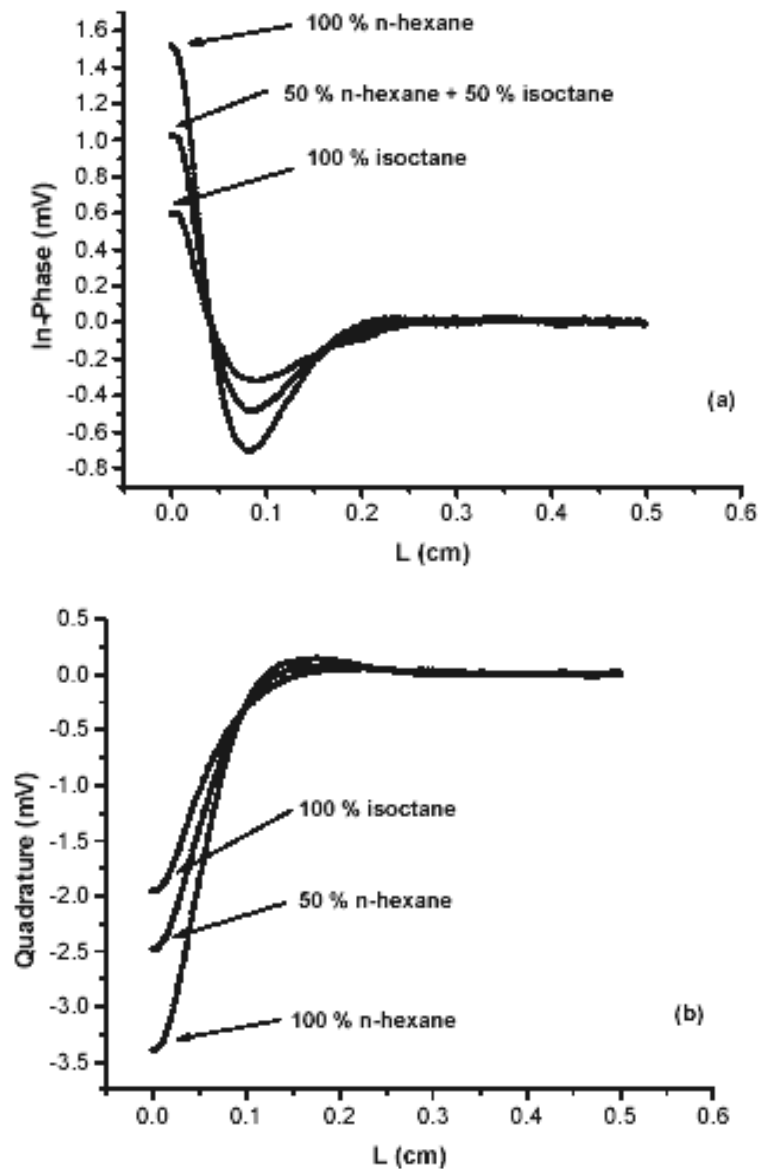


Figure 9. In-Phase and Quadrature signals as a function of the cavity length for mixtures of n-hexane and isooctane at different relative concentrations in the liquid phase (Taken from Ref. [76]).

approaching saturation and the thermal diffusivity of the saturated air-gasoline vapor mixture. The plot of the characteristic times versus the thermal diffusivity for 210 commercial samples collected in different gas stations is shown in Fig. 11. Non-adulterated gasoline samples data are represented by the open circles, whereas the adulterated samples data are shown by crosses. A conformity grid defined by the solid lines in the figure was defined taking the average values of both τ and α together with twice their standard deviations. Samples whose data fell outside the conformity grid were classified as the adulterated samples to an uncertainty of 5.7%.

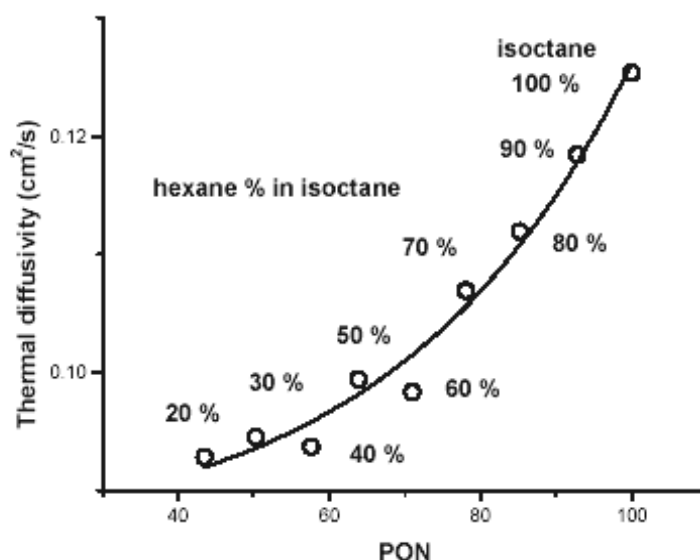


Figure 10. Thermal diffusivity versus Pump Octane Number for different concentrations of (liquid) *n*-hexane in isooctane. The solid curve is the best fit to an exponential growth function. (Taken from Ref. [76]).

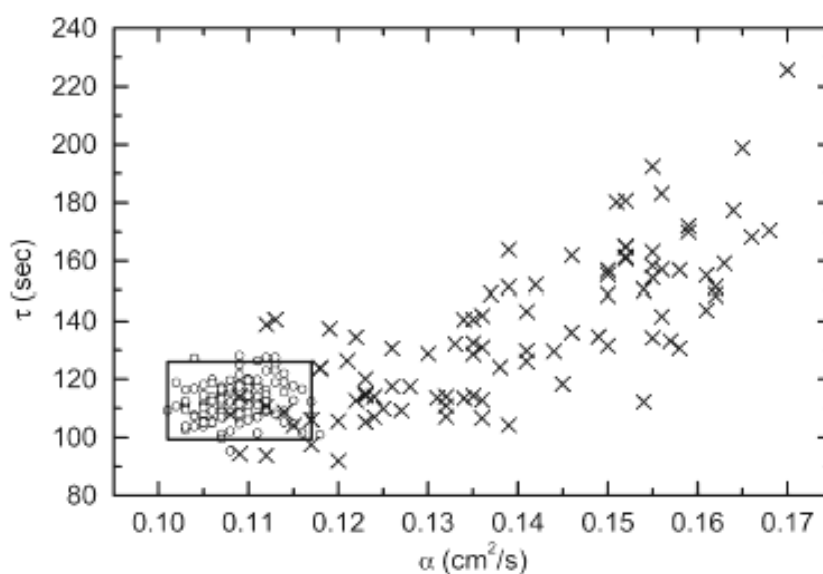


Figure 11. Correlation between the characteristic decay time and the thermal diffusivity for the 210 gasoline samples. The solid rectangle represents the conformity grid. Measurements were performed at 23°C, at $f=10$ Hz and $L=2$ mm (Reprinted in part with permission from Ref. [41]. Copyright 2004 American Chemical Society).

The explanation of the observed results was given using the kinetic theory of gases as follows: automotive fuels are commonly adulterated with light substances, such as, pentane, hexane, and ethanol, among others, available at low prices. The net effect of this would be a decrease of the effective mass of the resulting fuel vapor in the air/fuel vapor mixture, with a

consequent increase of the thermal diffusivity of the gaseous mixture and one would expect that the saturated air/adulterated fuel vapor mixture exhibits higher thermal diffusivity than the corresponding mixture with unadulterated fuels, as observed in the figure. Respecting the behavior of the characteristic time, the point to bear in mind is that it should depend not only on the nature of the constituent's gases, as in the case of the thermal diffusivity, but also on extensive parameters, such as the vapor concentration in the air/fuel vapor mixture. For fuels adulterated with high volatile light solvents, it seems plausible to expect a higher concentration of fuel vapor thereby leading to longer times, as was observed.

The good accuracy of the method, together with its simplicity and fast response, may render it useful for developing a portable device for fast checking in field analysis [80].

6. Conclusions and outlook

The here presented results not only try to fill the lack of discussion on some aspects in the field of thermal wave interferometry but also suggest a framework for investigating a wide range of applications ranging from measurements of transport properties (mass and thermal diffusion coefficients, thermal conductivity, and so on) to the study of time varying processes with potential use in the monitoring of soil and plants respiration kinetics and pollutant diffusion in ambient air, in addition to the applications mentioned in the last sections of this chapter. Thermal wave interference has fulfilled a great part of its expectative, since it was discovered and applied for the first time approximately two decades before. For the characterization of gases novel developments deserve special attention and much promising is the capability to construct compact devices, suitable for in-field measurements in several applications. This chapter should be a new step towards the understanding of the physical mechanisms behind thermal wave interference experiments with gases and to show and understand some of their applications.

Acknowledgements

The support of the Brazilian agencies CNPq and FAPERJ is greatly acknowledged. EM also thanks the postdoctoral program of CLAF-CNPq and the Alma Mater Project 012001 from Havana University for the partial support throughout early phases of his work on TWI at UENF, RJ, Brazil, as well as the support of SIP-IPN projects 20080032 and 20090160, SEP-CONACyT Grants 61-541 and 83-289 and COFAA-IPN, México, during the writing of this article.

References

1. Bennett, C. A. and Patty, R.R. 1982, *Appl. Opt.*, 21, 49.
2. Almond, D. P. and Patel, P. M. 1996, "Photothermal Science and Techniques" in "Physics and its Applications, 10", E.R. Dobbsand and S.B. Palmer (Eds), Chapman and Hall, London.
3. Cielo, P. and Dallaire, S. 1986, *J. Mater. Eng. Syst.* 9, 71.
4. Patel, P.M., Almond, D.P. and Morris, J.D. 1991, *Eur. J. NDT* 1, 64.
5. Bento, A.C., Brown, S.R., Almond, D.P. and Turner, I.G. 1995, *J. Mater. Sci.* 06, 335.
6. Bento, A.C. and Almond, D.P. 1995, *Meas. Sci. Technol.* 6, 1.
7. Bento, A.C., Almond, D.P., Brown S.R. and Turner, I.G. 1996, *J. Appl. Phys.* 79, 6848.
8. Almond, D.P., Patel, P.M, Pickup, I.M. and Reiter, H. 1985, *NDT Int.* 18, 17.
9. Patel, P.M. and Almond, P.M. 1985, *J. Mater. Sci.* 20, 955.
10. Coelho, T.M., Nogueira, E.S., Weinand, W.R., Lima, W.M, Steimacher, A., Medina, A.N., Baesso, M.L. and Bento, A.C. 2007, *J. of Appl. Phys.* 101, 084701.
11. Rosencwaig, A. and Gersho, A. 1976, *J. of Appl. Phys.* 47, 64.
12. Cielo, P. 1984, *J. Appl. Phys.* 56, 230.
13. Cielo, P., Lewak, R., Maldague, X. and Lamontagne, M. 1986 *C.S.N.D.T. Journal* 7, 2.
14. Parker, W.J., Jenkins, R.J., Butler, C.P. and Abbott, G.L. 1961 *J. Appl. Phys.* 32, 1679.
15. Lau, S.K., Almond, D.P. and Patel, P.M. 1991, *J. Phys. D: Appl. Phys.* 24, 428.
16. Depriester, M., Hus, P., Delenclos, S, and Hadj Sahraoui 2005, *Rev. Sci. Instrum.*, 76, 074902.
17. Nzodoum Fotsing, J.L., Gibkes, J., Pelzl, J. and Bein, B.K. 2005, *J. Appl. Phys.* 98, 063522.
18. Shen, J. and Mandelis, A. 1995, *Rev. Sci. Instrum.*, 66, 4999.
19. Shen, J., Mandelis, A. and Aloysius, B.D. 1996, *Int. J. Thermophys.* 17, 1241.
20. Shen, J., Mandelis, A. and Ashe, T. 1998, *Int. J. Thermophys.* 19, 579.
21. Mandelis, A. and Matvienko, A. 2007, "Photopyroelectric thermal-wave cavity devices-10 years later" in *Pyroelectric Materials and Sensors*", D. Rémiens (Ed.) Research Signpost, Kerala, India, 61.
22. Pan, G and Mandelis, A. 1998, *Rev. Sci. Instrum.* 69, 2918.
23. Matvienko, A. and Mandelis, A. 2005, *Int. J. Thermophys.* 26, 837.
24. Shen, J, Mandelis, A. and Tsai, H. 1998, *Rev. Sci. Instrum.* 69, 198.
25. Wang. C. and Mandelis, M. 1999 *Rev. Sci. Instrum.* 70, 3115.
26. Lima, J.A.P., Marín, E., Correa, O., Cardoso, S., da Silva, L. M.G., Vargas, H. and Miranda, L.C.M. 2000, *Meas. Sci. Technol.*, 11, 1522.
27. Lima J. A. P., Marín E., Cardoso S. L., Takeuty D., da Silva M. G., Sthel M. S., Rezende C. E., Gatts C. N., Vargas H. and Miranda L.C.M. 2000, *Rev. of Sci. Inst.* 71, 2928.

28. Esquef, I.A., Siqueira, A.P., da Silva, M.G., Vargas, H. and Miranda, L.C.M. 2006, *Anal. Chem.* 78, 5218.
29. Lima, C.A.S., Miranda, L.C.M. and Vargas, H. 2006, *Instrum. Sc. Technol.* 34, 191.
30. Delenclos, S., Dadarlat, D., Houriez, N., Longuemart, S., Kolinsky, C., and Hadj Sahraoui, A. 2007, *Rev. Sci. Instrum.* 78, 024902.
31. Lima J.A.P., Marín E., da Silva M. G., Sthel M. S., Schramm D. U., Cardoso S. L., Vargas H. and Miranda L. C. M. 2001, *Meas. Sci. Technol.*, 12, 1949.
32. Lima J.A.P., Marín E., Cardoso S. L., da Silva M.G., Sthel M.S., Vargas H. and Miranda L.C.M. 2001, *Rev. Sci. Instrum.* 72, 1580.
33. Lima J.A.P., Marín E., Massunaga M.S.O., Correa O., Cardoso S.L., Vargas H. and Miranda L.C.M. 2001, *Appl. Phys. B: Lasers and Optics* 73, 151.
34. Marin E., Lima J. A. P., da Silva M. G., Sthel M. S., Cardoso S. L. and Vargas H. *Analytical Sciences* 17 475 (2001).
35. Lima, J.A.P., da Silva, M G, Massunaga, M.S.O., Marín, E., Vargas, H. and Miranda, L.C.M. 2002, *J. Appl. Phys.* 91, 5581.
36. Lima, J.A.P., da Silva, M.G., Sthel, M.S., Cardoso, S.L., Vargas, H., Marin, E. and Miranda, L.C.M. 2003, *Rev. Sci. Instrum.* 74, 433.
37. Lima, J.A.P., da Silva, M G, Massunaga M.S.O., Cardoso, S. L., Vargas, H., Marín, E. and Miranda, L.C.M. 2003, *Rev. Sci. Instrum.* 74, 842.
38. Balderas-López, J. A. and Mandelis, A. 2001, *J. Appl. Phys.* 90, 3296.
39. Bonno, B., Laporte, J.L. and Tascon D'Leon, R. 2005, *Rev. Sci. Instrum.* 76, 096104.
40. Balderas-López J. A, Mandelis A. and García J. A. 2001, *Anal. Sci.* 17, 519.
41. Lima, J.A.P., Massunaga, M.S.O., Vargas, H. and Miranda, L.C.M. 2004, *Anal. Chem.* 76, 114.
42. Burgess D. S., *Photonics Technology World*, March 2004.
43. Rosencwaig, A. 1975 *Physics Today* 28, 23.
44. Rosencwaig, A. 1980 *Photoacoustics and Photoacoustic Spectroscopy*. Wiley, New York.
45. Viengerov, M. L. 1938 *Dokl. Akad. Nauk. SSSR* 19, 687.
46. Sigrist M.W. 1994 In "Air Monitoring by Spectroscopic Techniques" M.W. Sigrist (Ed.) Wiley, New York, 163.
47. de Vries, H.S.M. 1995 "Non-intrusive fruit and plant analysis by laser photothermal measurements of ethylene emission" In "Modern methods of plant analysis" H.F. Linskend and J.F. Jackson (Eds) Springer-Verlag, Heidelberg.
48. *Pyroelectric Materials and Sensors 2007*, D. Rémiens, D. (Ed.) Research Signpost, Kerala, India.
49. Pessoa Jr, O., Cesar, C.L., Patel, N.A., Vargas, H., Ghizoni, C.C. and Miranda, L.C.M. 1986 *J. Appl. Phys.* 59, 1316.
50. Perondi, L.F. and Miranda, L.C.M. 1987 *J. Appl. Phys.* 62, 2955.
51. Marquezini, M.V., Cella, N., Manzanares, A.M., Vargas, H. and Miranda, L.C.M. 1991 *Meas. Sci. Technol.* 2, 396.
52. Marín, E., Vargas, H., Diaz, P. and Riech, I. 2000 *Phys. Stat. Sol.(A)* 179, 387.
53. Reguera, E., Marín, E., Calderón, A. and Rodríguez-Hernández, J. 2007 *Spectrochimica Acta A: Mol. Biomol. Spectrosc.* 68, 191.

54. Bertolotti, M., Li Voti, R., Liakhov, G.L., Paolini, S. and Sibilina, C. 1999 in Photoacoustic and Photothermal Phenomena: 10th International Conference. F. Scudieri and M. Bertolotti (Eds.) The American Institute of Physics, 96.
55. Murphy, J.C. and Aamodt, L.C. 1980 J. Appl. Phys. 51, 4580.
56. Bein, B.K. and Pelzl, J. 1989 "Analysis of Surfaces exposed to Plasmas by Nondestructive Photoacoustic and Photothermal Techniques" in "Plasma Diagnostics, Surface Analysis and Interactions" Academic, New-York, 211.
57. Marin, E. 2007 Eur. J. Phys. 28, 429.
58. Mandelis, A. 2001, Diffusion-wave fields: mathematical methods and green functions. Springer-Verlag New York.
59. Mandelis, A, Vanniasinkam, J., Budhudu, S., Othonos, A. and Kokta, M. 1993, Phys. Rev. B 48, 6808.
60. Chirtoc, M., Chirtoc, I., Bicanic, D. and Pelzl, J. 1995 Ferroelectrics 165, 27.
61. Christofides, C., Mandelis, A., Gandhi, K. and Wagner, R. E. 1990, Rev. Sci. Instrum. 61, 2360.
62. Thoen, J. and Glorieux, C. 1997 Thermochemica Acta 304/305, 137.
63. Dadarlat, D., Riezeos, K.J., Bicanic, D., van den Berg, C., Gerkema, E. and Surducun, V. 1998 Adv. Food Sci. (CMTL) 20, 27.
64. Dadarlat, D., Bicanic, D., Visser, H., Mercuri, F. and Frandas, A. 1995 JAOCS 72, 281.
65. Favier, J.P., Dadarlat, D., Gibkes, J., van den Berg, C. and Bicanic, D. 1998, Inst. Sc. and Technol. 26, 113.
66. Touloukian Y.S., Powel, R.W., Ho, Y.C., Nocalasu, M.C. 1973 Thermal diffusivity, Plenum, New York.
67. Touloukian Y.S. (Ed.) 1970, Thermophysical Properties of Matter. The Thermophysical Properties Research Center Data Series, IFI/Plenum Press, New York.
68. Srivastava B. N. and Saxena S. C. 1957, J. Chem. Phys. 27, 583.
69. Tye R. P. 1969, Thermal Conductivity Vol. 1. Academic, New York.
70. Kothandaraman, C.P. and Subramanyan, S. 1977 Heat and Mass Transfer Data Book, Wiley, New York.
71. Whitaker, S. 1976 Elementary Heat Transfer Analysis, Pergamon, New York.
72. Lyde, D. (Ed.) 1995 Handbook of Chemistry and Physics, 75th ed, Chemical Rubber Co, Cleveland.
73. Reid, R.C., Praunitz, J.M. and Poling, B.E. 1987 The properties of Gases and Liquids, 4th ed., McGraw-Hill, New York.
74. Crank, J. 1975 The mathematics of diffusion. Clarendon, Oxford.
75. Yaws, C.L. 1995, Handbook of Transport Properties Data: Viscosity, Thermal Conductivity and Diffusion Coefficients. Gulf, Houston.
76. Cardoso, S.L, da Silva, M.G., Lima, J.A.P. Sthel, M.S., Marin, E. and Vargas, H. 2001 Anal. Sc. 17, 479.
77. Lima, J.A.P., Cardoso, S.L., da Silva, M.G., Sthel, M.S., Gatts, C.E.N and Vargas, H. 2001 Ind. Eng. Chem. Res. 40, 6207.
78. D2699-99 Standard Test Method for Research Octane Number of Spark-Ignition Engine Fuel. American Society for Testing and materials, PA, USA.

79. D2700-99 Standard Test Method for Motor Octane Number of Spark-Ignition Engine Fuel. American Society for Testing and materials, PA, USA.
80. Lima, J.A.P. System for the measure of the thermal properties of fluids. United States Patent 20070288193.